Collisional-Radiative Modeling for Highly-Charged Ions of Tungsten*)

Yuri RALCHENKO

National Institute of Standards and Technology, Gaithersburg MD 20899-8422, USA

(Received 10 December 2012 / Accepted 5 February 2013)

We present an overview of the recent advances in collisional-radiative modeling of highly-charged ions of tungsten that are relevant to fusion research. The status of spectroscopic data for W ions is briefly discussed as well. Strategies and peculiarities of building models for Maxwellian fusion plasmas and non-Maxwellian plasmas of electron beam ion traps are outlined. Comparisons with the measured x-ray and extreme ultraviolet spectra are also given.

Keywords: tungsten, spectra, collisional-radiative modeling, highly-charged ion

DOI: 10.1585/pfr.8.2503024

1. Introduction

Spectroscopy of highly-charged ions of tungsten has become a significant and highly visible component of atomic physics research over the last decade. This development is influenced by the planned usage of tungsten as a plasma-facing material in the ITER divertor [1]. Its exceptional thermophysical properties as well as low tritium retention make tungsten one of the best materials to withstand high thermal loads in fusion plasmas. However, even at the core plasma temperatures of 15-20 keV, W ions will not be completely ionized and thus give rise to undesirable radiative power losses. This for instance puts substantial limitations on the allowed concentration of W in the ITER core.

Since tungsten will practically be the only non-fully-ionized element in the plasma core, its spectra may serve as an accurate diagnostic tool. Several experimental programs are actively involved in analysis of tungsten spectra, and the number of spectroscopic papers on W produced over the last 10-15 years is too large to list here. Such fusion devices as ASDEX Upgrade [2], LHD [3], JT-60U [4], Alcator C-Mod [5] and others are being used to produce and study spectra from various ions of tungsten. These analyses have resulted in identification of a large number of spectral lines. In addition to fusion devices, spectra of highly-charged ions of tungsten are studied in z-pinches [6] and especially electron beam ion traps (EBITs) [7–13], the latter having become a de facto primary source of data on energy levels and spectral lines. A localized plasma volume, absence of transport effects, stability of operation, and ability to produce practically any ion of any element make EBITs one of the best choices to study highly-charged ions. One of the important steps in analysis and identification of EBIT spectra is the collisional-radiative (CR) modeling. CR models use information on physical processes affecting level populations to calculate spectra under specific plasma conditions. In this paper we present a brief review of collisional-radiative modeling for highly-charged tungsten produced in EBIT and fusion plasmas, with the emphasis on the research performed at the National Institute of Standards and Technology (NIST).

2. Spectroscopic Data for W

The intensity of a spectral line due to a radiative transition from the upper level j to the lower level i in an optically thin plasma is defined as:

$$I_{ij}(\lambda) = N_j \cdot A_{ij} \cdot E_{ij} \cdot \varphi(\lambda), \tag{1}$$

where λ is the wavelength, N_j is the population of the upper level, A_{ij} is the transition probability or Einstein coefficient, $E_{ij} = hc/\lambda$ is the transition energy, and $\varphi(\lambda)$ is the normalized line profile. The latter may include contributions from Doppler, natural, collisional and instrumental broadenings, and will not be discussed here. In low- to mid-density fusion plasmas both transition probability and transition energy are not modified by the plasma environment and thus can be safely determined from "standard" isolated-atom experiments, available atomic databases, or even high-precision atomic structure calculations. The populations, on the other hand, are determined by the emitter interaction with plasma particles and therefore to calculate N_j one has to analyze all important collisional and radiative processes affecting the level populations. This task obviously depends on the specific plasma conditions and will be the main subject of this review.

Critical compilations of energy levels and spectral lines for all ions of tungsten were reported in the recent papers by Kramida and Shirai [14, 15]. The authors thor-

author's e-mail: yuri.ralchenko@nist.gov

*) This article is based on the invited presentation at the 22nd International Toki Conference (ITC22).

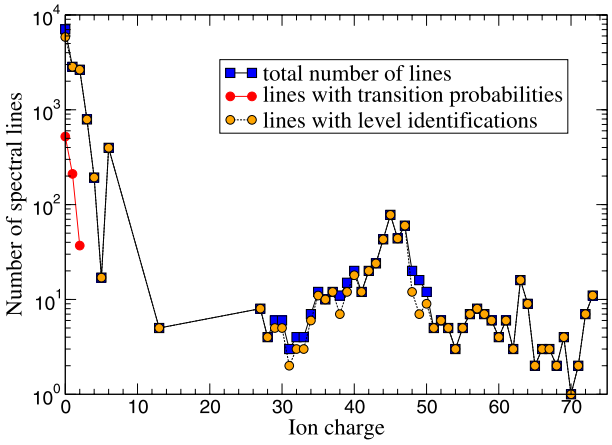

Fig. 1 Spectral line data for W ions available in the NIST Atomic Spectra Database (as of November 2012).

oughly analyzed the available experimental data from various sources and produced recommended sets with evaluated uncertainties. For some ions (e.g., He- and H-like W) highly accurate theoretical results were compiled. These compilations provide spectroscopic information on energies of atomic levels and their wavefunction composition, observed and Ritz wavelengths, and the related data uncertainties. Recently Kramida published an update on the progress in tungsten spectroscopy [16] that contains details on spectra measurements and analyses produced after 2007. These publications also contain the ionization potentials for all ions of tungsten that are mainly based on Ref. [17].

All recommended spectroscopic data for tungsten can be found in the NIST Atomic Spectra Database (ASD) [18]. As of November 2012, NIST ASD contains 2229 energy levels and 14510 spectral lines for all ions from neutral tungsten with 74 electrons to H-like one-electron ion W^{73+}. The distribution of the spectral line data over ionization stages is shown in Fig. 1. Most of the data are available for the neutral and lowest ions, for higher ions the number of known lines and levels is generally small. For some ions (W VIII-W XIII, W XV-W XXVII) ASD contains no spectroscopic data primarily due to difficulties in reliable identification of the few measured complex spectra. Currently several groups are working on production and identification of W spectra from low- and mid-charge ions so that hopefuly these gaps will soon be filled to some extent.

3. Collisional-Radiative Modeling of EBIT Spectra

EBIT is a relatively small, typically table-top-sized device with a Penning trap, electron beam, and gas or metal injection system being its primary components (see, e.g., [19]). Highly-charged ions are produced by the beam, its field is also used to confine the ions along with the strong magnetic field of the trap. EBITs are rather inexpensive, can be purchased from commercial companies, and are currently used in numerous laboratories and institutions around the world.

The plasma conditions inside EBITs differ from those in fusion devices in several aspects. The electron density in EBITs is lower by one or two orders of magnitude, and the ion temperature is very low as compared to tokamaks. From the CR modeling point of view, however, the principal difference is in the electron energy distribution function (EEDF) which is typically a Maxwellian one in fusion machines and a very narrow (quasi-)Gaussian in EBITs. In fact, for most applications it is even safe to consider an EBIT EEDF as a δ-function. This difference is, for instance, exhibited in such an important physical process as dielectronic recombination (DR). DR is a two-step process, first step being the dielectronic capture, i.e., capture of a free electron with simultaneous excitation of an atomic electron, that is then followed by the radiative stabilization. This process is a resonant one and for it to proceed, a beam electron must have an exact energy required for dielectronic capture. Of course, this is not generally the case. Accordingly, DR may be ignored in EBIT studies unless it is accidentally or intentionally produced in a particular experiment. In a Maxwellian plasma, however, there always exist electrons with any energy and hence DR is always possible and must be included in simulations.

Spectra modeling becomes relatively simple for high densities when plasma are in local thermodynamic equilibrium (LTE). When collisions in a Maxwellian plasma are much stronger than radiative processes, populations of atomic levels and ionization stages are distributed according to the Saha-Boltzmann formulas that, in addition to electron temperature, depend only on energies and statistical weights. In this case, no information on collisional cross sections, which are the most difficult and time-consuming data to calculate, is required; the line intensities can be simply calculated from the Boltzmann distribution and Einstein coefficients. However, high densities often imply importance of opacity effects that affect the spectra. Since the most important radiative transitions, namely, the electric-dipole ones, have a strong dependence on ion charge $A \propto Z^4$, and the collisional $\Delta n \geq 1$ rate coefficients decrease as $\langle \sigma v \rangle \propto Z^{-3}$, the typical electron densities required to reach LTE increase as Z^7. Therefore, a complete Saha-Boltzmann equilibrium for ions of tungsten with $Z \sim 50$ can be reached only at exceedingly large densities above $10^{26}\,\mathrm{cm}^{-3}$. Moreover, some plasmas used to study highly-charged heavy ions, e.g., those in EBITs, are intrinsically non-Maxwellian and thus LTE considerations are not applicable to them.

The low-density limit for level population and spectra modeling, the coronal approximation, assumes that atomic levels are populated by either direct excitations from the ground state or radiative cascades from the higher excited states. Generally, this is a rather good approach for the

strongest lines in EBITs, however, important diagnostic features for weaker forbidden lines cannot be adequately analyzed within the coronal model.

The collisional-radiative model [20] takes into account the most important physical processes to build and solve a system of rate equations for level populations for arbitrary densities. In the low- and high-density limits, this model converges to the coronal and Saha-Boltzmann approximations, respectively. Even within a general CR approach, different models can be developed based on different structure description for the included ions. Thus, one can build a model where atomic states are atomic levels, terms in LS- or jj-coupling, configurations, superconfigurations, even average atoms. It is becoming customary these days to develop hybrid models where lower states are represented in much detail (e.g., as fine-structure levels) while higher excited states are described using more general presentations (e.g., terms or configurations). A particular choice of the model structure depends on a specific problem to be addressed: for instance, for ionization balance studies a generalized description would suffice while for spectroscopic diagnostics one has to have as detailed description of the emitting states as possible.

Typically, the physical processes included in CR models are spontaneous radiative transitions, electron-impact processes (excitation, deexcitation, and ionization), autoionization (if autoionizing states are explicitly included), three-body and radiative recombination, and dielectronic recombination. The latter process can be introduced via general ion-to-ion rates or, in a more detailed approach, via dielectronic capture into autoionizing states followed by radiative stabilization. Depending on plasma conditions, some other processes ought to be added, such as charge exchange with neutral beams in fusion devices or with background neutrals in EBITs. A CR model can be readily extended to include interaction with external radiation fields, and therefore it is widely used in analysis of photoionized astrophysical plasmas. More advanced CR models can also account for ionization potential lowering in dense plasmas, opacity effects via escape factor approximation or detailed radiative transport, or motional Stark effect via introduction of parabolic m-resolved states [21].

A key component of any CR model is the atomic data on structure, radiation, and collisions. It is very rare that the available atomic data in the existing databases can provide a sufficiently complete set of parameters for modeling. Thus, CR simulations are to begin with calculation of energy levels, radiative transition probabilities, and collisional cross sections (or rate coefficients). For relatively high-charged ions, the Flexible Atomic Code (FAC) [22] has become one of the widely used atomic packages, and we implement it extensively for our data needs. The wavefunctions are calculated with the relativistic model-potential method accounting for configuration interaction and intermediate coupling. It is also important to include not only the allowed electric-dipole (E1) radiative transitions but also the forbidden multipole transitions of higher orders, such as magnetic-dipole (M1) or electric-quadrupole (E2) ones. The probabilities of forbidden transitions increase with ion charge much faster than those for E1 transitions, and therefore forbidden lines become very prominent for highly-charged ions. The electron-impact cross sections can be calculated with the relativistic distorted-wave approximation or the Coulomb-Born method which offer good accuracy for high Z.

The details and structure of a specific CR model should depend on the physical problem under consideration since it would be computationally prohibitive to develop a general universal CR model applicable to all possible plasma environments and spectral features. For instance, if one studies $\Delta n \geq 1$ x-ray transitions, the details of the initial excited states of transitions should be fully included in the model. On the other hand, for analysis of forbidden transitions within the ground configuration a detailed representation of higher excited states is not crucial (see below).

The atomic data generated with FAC are then used to create a database for the collisional-radiative code NOMAD [23] that calculates ionization distributions, level populations, and spectral line intensities. Since the NOMAD database contains collisional cross sections rather than rate coefficients, this code can be used for both Maxwellian plasmas of fusion devices and non-Maxwellian plasmas in EBITs.

One of the first tungsten-related experiments on the NIST EBIT addressed the outstanding problem from ASDEX Upgrade x-ray measurements at $T_e \approx 4\,\mathrm{keV}$ [24, 25]. One of the spectral lines at 7.93 Å, which was associated with an E2 transition in Ni-like W, was found to have the intensity much higher than predicted from several CR calculations. Using an x-ray microcalorimeter, a tungsten EBIT spectrum was measured between 3 Å and 10 Å at the beam energy of 4 keV [12]. Figure 2 shows the experimental spectrum (top) and the NOMAD simulations (bottom). An excellent agreement between two spectra is in part due to the fact that almost all spectral lines originate from a single ion, the Ni-like W^{46+}. Nonetheless, one can clearly see that the intensity of the forbidden line at 7.93 Å is reproduced very well at the EBIT electorn density of $n_e \sim 10^{12}\,\mathrm{cm}^{-3}$. It turns out that this line is an overlap of electric-quadrupole (E2) and magnetic-octupole (M3) lines with very close wavelengths and the predicted intensity ratio of approximately 4:3. Neither the spectral resolution of our microcalorimeter nor that of the spectrometers used in Refs. [24, 25] were high enough to separate these lines. Later, however, E2 and M3 lines were resolved with a high-resolution x-ray spectrometer [26], and the measured line intensity ratio agreed with our predicted value.

The CR model for non-Maxwellian EBIT spectra was then applied to the typical conditions of Maxwellian fusion plasmas. It was found [27] that with the increase of elec-

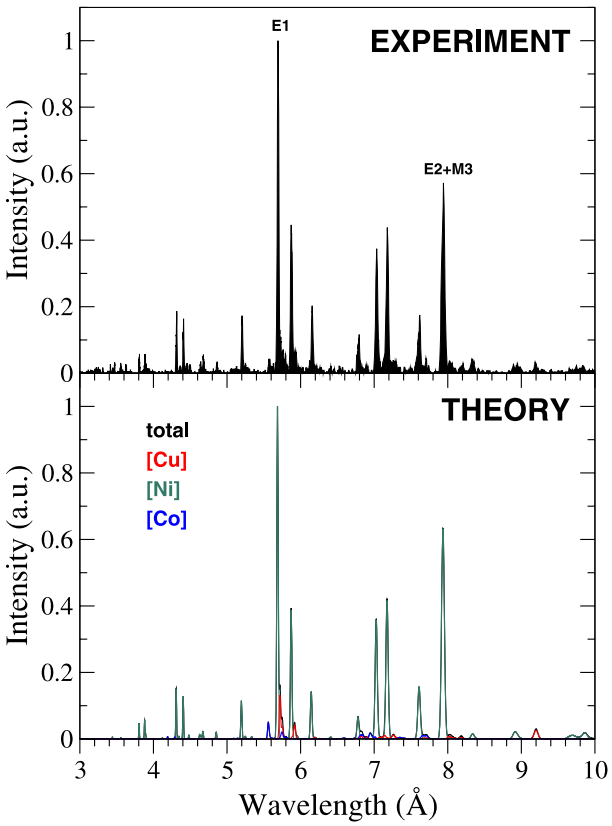

Fig. 2 Comparison of the measured (top) and calculated (bottom) spectra of W at 4 keV [12]. The bottom plot shows separate contributions to the spectrum from the most abundant ions of W.

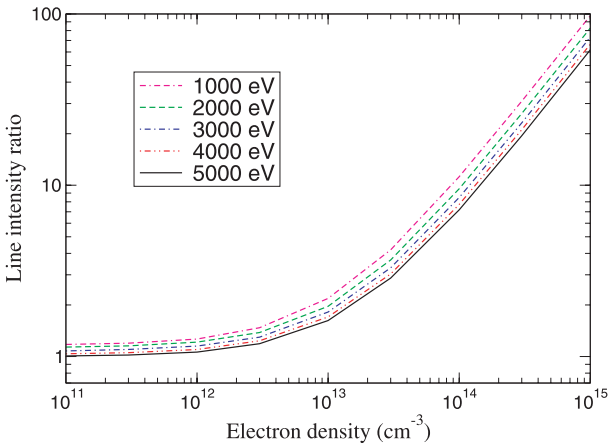

Fig. 3 Density-dependent line intensity ratio of the electric-quadrupole to magnetic-octupole lines in Ni-like W^{46+} [12] for electron temperature between 1000 eV and 5000 eV.

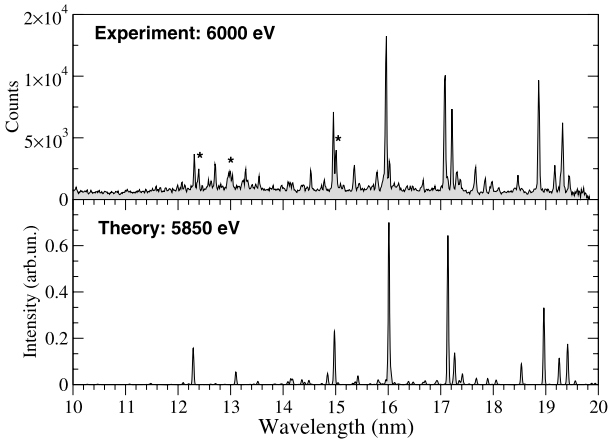

Fig. 4 Comparison of experimental and theoretical spectra for W in the EUV spectral range. Impurity lines are marked by asterisks. All strong lines in this spectrum are due to the forbidden magnetic-dipole transitions within $3d^n$ ground configurations.

tron density, population from the M3 level is transferred to the E2 level via collisions followed by radiative decays. Therefore, the intensity of M3 line decreases while that of the E2 line increases with density, and thus the ratio of two lines can be used as a good diagnostic of electron density (Fig. 3). Interestingly, the total intensity of the unresolved E2+M3 spectral feature at 7.93 Å remains practically constant over a large range of n_e.

The size of a model, that is, the number of included states, can vary depending on the included ions. For ions with/near the closed-shell ground configuration, the number of states per excitation is relatively small. However, for ions with a large number of electrons in an open shell, even single excitations result in a very large number of possible states. In this case, a practical method to reduce the size of the rate matrix is to use some version of a hybrid approach. In our recent study of the $3d^n$ ions of tungsten [9], the $n = 3$ single and double excitated states were represented as atomic levels, while the $n \geq 4$ levels were combined into "superterms" characterized by the total angular momenta of the relativistic subshells of the atomic core $3d$. This approach allowed us to significantly reduce the rate matrix size and speed up the calculations. An example of agreement between the measured extreme ultraviolet (EUV) spectrum at the beam energy of 6 keV and the calculated spectrum at 5.85 keV is given in Fig. 4. The small difference in the nominal and theoretical energies is due to the space charge effect that can well be accounted for. All strong spectral lines in Fig. 4 are due to the forbidden M1 transitions within the ground $3d^n$ configurations of approximately 50-times ionized tungsten.

Similar to the E2/M3 ratio discussed above, the M1 lines in $3d^n$ ions also exhibit sensitivity to electron density. To this end, we performed Maxwellian simulations for a large range of densities and found about two dozen line pairs that are indeed density-sensitive. An example is presented in Fig. 5. These lines are due to EUV magnetic-dipole transitions within the $3d^6$ ground configuration of Cr-like W^{50+}. At low densities $n_e \lesssim 10^{13}$ cm^{-3}, the collisional destruction times due to electron-impact (de)excitation are longer than the corresponding radia-

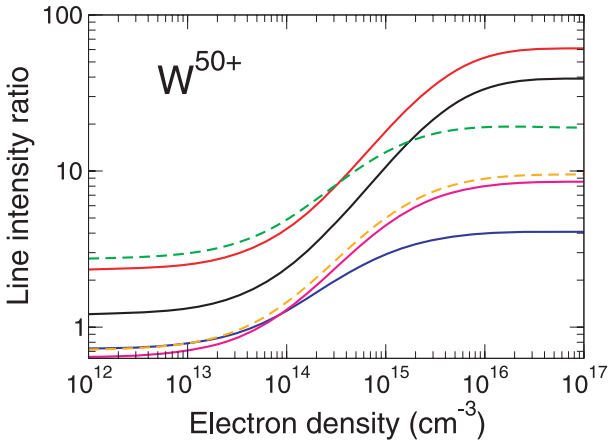

Fig. 5 Line intensity ratios for several pairs of magnetic-dipole lines within the $3d^6$ ground configuration of Cr-like W^{50+}.

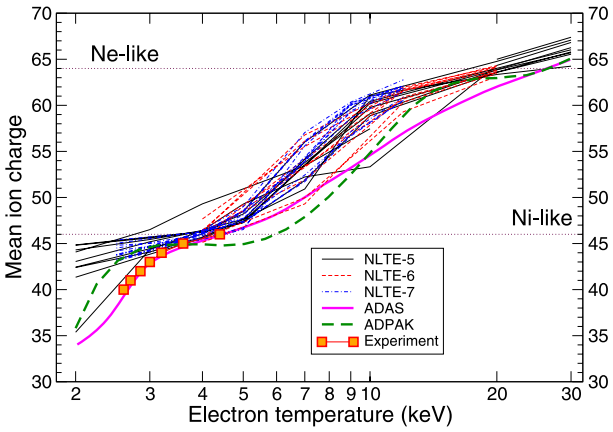

Fig. 6 Mean ion charge of W at electron density $N_e = 10^{14}$ cm^{-3} from NLTE Workshop simulations. Experimental data: Ref. [25]; ADAS: Ref. [2]; ADPAK: Ref. [31].

tive lifetimes and therefore all excited electrons decay radiatively resulting in density-independent line ratios. At higher densities, the lines with low transition probabilities are collisionally destroyed thereby resulting in n_e-dependent ratios with stronger lines. Importantly, the shown lines originate from the same ionization stage and thus are not sensitive to ionization balance.

4. Tungsten Simulations at NLTE Workshops

A very successful series of workshops on validation and verification of collisional-radiative models, the Non-Local Thermodynamic Equilibrium (NLTE) Code Comparison Workshops, has been held since 1996 [28]. The primary goal of these meetings is to pinpoint and analyze differences between various CR models. This is achieved through (i) "homework" CR calculations for identical plasma conditions characterized by particle density and temperature, and (ii) comparison of different population kinetics parameters (e.g., mean ion charges, ionization distributions, and rate coefficients). Such comparisons may include both steady-state and time-dependent problems and various plasma effects (finite plasma size, opacity, ionization potential lowering, etc.) while more complex issues (e.g., ion transport) are left for future meetings. This series of workshops has in fact become one of the primary forums for the CR modelers.

While the first NLTE workshops mostly addressed population kinetics of rather dense ($n_e \gtrsim 10^{20}$ cm^{-3}) plasmas, the growing importance of tungsten in magnetic fusion resulted in addition of W cases at $n_e = 10^{14}$ cm^{-3}. At the NLTE-5 workshop [29, 30], calculations from ten different codes for tungsten at electron temperatures between 2500 eV and 30 keV were first presented and discussed in much detail. The next two workshops, results of which have not been published yet, focused on the lower half of this temperature range. An example of calculations is presented in Fig. 6 where the mean ion charge $\overline{Z}$ for W ions is shown for $n_e = 10^{14}$ cm^{-3}. The experimental values are inferred from the ASDEX Upgrade measurements [25]. A visibly good agreement between the ADAS calculations presented by a thick (magenta) curve [2] and the measured data is due to ad hoc corrections to ADAS recombination rates; these modifications were obtained by fitting the experimental results. All NLTE Workshop results, however, are purely *ab initio* calculations without any empirical corrections. Figure 6 also shows the old calculations with the averaged ion model [31].

As follows from the figure, practically all codes converge to $Z = 46$ at about 4 keV and to $Z = 64$ at about 20 keV. These ion charges correspond to the closed-shell $3d^{10}$ Ni-like W^{46+} and $2p^6$ Ne-like W^{64+} ions. Unlike other codes, the ADAS results at the ITER core temperature of 20 keV show somewhat smaller mean ion charge, ~62. This difference increases in the intermediate temperature range of 5-15 keV where M-shell ions are most abundant. For instance, most of the codes have $\overline{Z}$ close to 58 at 9 keV while the ADAS value is 53. Even more significant difference is observed at lowest temperatures $T_e \lesssim 3$ keV reaching almost ten units at 2 keV. At these temperatures, the most abundant ions are those with an open N shell ($n = 4$) which are very difficult to model due to a large number of excited states to be included in simulations. Yet it is clear that all codes participating in the NLTE workshops approximately agree within ±2 units of ion charge even for such complex ions. This discrepancy calls for new independent measurements of tungsten ionization balance between 2 keV and 4 keV.

5. Conclusions

The achievements in spectroscopy of highly-charged ions of tungsten over the last decade are numerous. The basic spectroscopic data, e.g., energy levels and spectral line wavelengths, are available for most of W ions although

there still exist significant gaps. Collisional-radiative modeling of tungsten spectra and kinetics has also advanced significantly due to development of accurate atomic and kinetic codes and benchmark spectroscopic measurements from electron beam ion traps. The agreement between modeling and EBIT measurements was instrumental in identification of a large number of spectral lines and in development of new diagnostic techniques for fusion plasmas. Hopefully, new precision experiments on fusion devices, which are still relatively rare, will be conducted in the near future and thus provide more realistic benchmarks to validate CR models for tungsten.

6. Acknowledgments

This work is supported in part by the Office of Fusion Energy Sciences of the U.S. Department of Energy. Valuable discussions with J.D. Gillaspy, J. Reader, D. Osin, A. Kramida, I.N. Draganić, J.N. Tan, J.M. Pomeroy and the participants of the Non-LTE Code Comparison Workshops are cordially acknowledged.

[1] R.J. Hawryluk *et al.*, Nucl. Fusion **49**, 065012 (2009).
[2] T. Pütterich *et al.*, Nucl. Fusion **50**, 025012 (2010).
[3] C. Suzuki *et al.*, J. Phys. B **44**, 175004 (2011).
[4] J. Yanagibayashi *et al.*, J. Phys. B **43**, 144013 (2010).
[5] A.T. Graf *et al.*, Can. J. Phys. **89**, 615 (2011).
[6] G.S. Osborne *et al.*, Can. J. Phys. **89**, 599 (2011).
[7] S.B. Utter *et al.*, Can. J. Phys. **80**, 1503 (2002).
[8] J. Clementson *et al.*, Can. J. Phys. **89**, 571 (2011).
[9] Yu. Ralchenko *et al.*, Phys. Rev. A **83**, 032517 (2011).
[10] J.D. Gillaspy *et al.*, Phys. Rev. A **80**, 010509 (2009).
[11] Yu. Ralchenko *et al.*, J. Phys. B **41**, 021003 (2008).
[12] Yu. Ralchenko *et al.*, Phys. Rev. A **74**, 042514 (2006).
[13] H. Watanabe *et al.*, Can. J. Phys. **90**, 497 (2012).
[14] A.E. Kramida and T. Shirai, J. Phys. Chem. Ref. Data **35**, 423 (2006).
[15] A.E. Kramida and T. Shirai, At. Data Nucl. Data Tables **95**, 305 (2009); Erratum: **95**, 1051 (2009).
[16] A.E. Kramida, Can. J. Phys. **89**, 551 (2011).
[17] A.E. Kramida and J. Reader, At. Data Nucl. Data Tables **92**, 457 (2006).
[18] A. Kramida, Yu. Ralchenko, J. Reader and NIST ASD Team, (2012). NIST Atomic Spectra Database (version 5.0), (Online). Available: http://physics.nist.gov/asd (Tuesday, 27-Nov-2012). National Institute of Standards and Technology, Gaithersburg, MD.
[19] J.D. Gillaspy, Phys. Scr. **T71**, 99 (2001).
[20] D.R. Bates, A.E. Kingston and R.W.P. McWhirter, Proc. R. Soc. Lond. **267**, 297 (1962).
[21] O. Marchuk, Yu. Ralchenko, R.K. Janev *et al.*, J. Phys. B **43**, 011002 (2010).
[22] M.F. Gu, Can. J. Phys. **86**, 675 (2007).
[23] Yu.V. Ralchenko and Y. Maron, J. Quant. Spectr. Rad. Transfer **71**, 609 (2001).
[24] R. Neu *et al.*, Phys. Scr. **T92**, 307 (2001).
[25] T. Pütterich *et al.*, Plasma Phys. Control. Fusion **50**, 085016 (2008).
[26] J. Clementson *et al.*, Phys. Rev. A **81**, 012505 (2010).
[27] Yu. Ralchenko, J. Phys. B **40**, F175 (2007).
[28] R.W. Lee, J.K. Nash and Yu. Ralchenko, J. Quant. Spectr. Rad. Transfer **58**, 737 (1997).
[29] C.J. Fontes *et al.*, High En. Dens. Phys. **5**, 15 (2009).
[30] Yu. Ralchenko *et al.*, AIP Conf. Proc. **1116**, 242 (2009).
[31] D. Post *et al.*, At. Data Nucl. Data Tables **20**, 397 (1977).